
Solution of a Dynamic Main Crack Interaction with a System of Micro-Cracks by the Element Free Galerkin Method

Boris Muravin^{1,2}, Eli Turkel¹, and Gregory Muravin²

¹ School of Mathematical Sciences, Department of Applied Mathematics, Tel-Aviv University, Tel-Aviv 69978, Israel. Tel: +972-3-6408038, Fax: +972-3-6409357.

² Margan Physical Diagnostics Ltd., P.O.B. 8155, Ha-Omanut 12, Netanya 42160, Israel. Tel: +972-9-8655510, Fax: +972-9-8655514, e-mail: bm@margan.com

Summary. Damage and failures in high-pressure equipment and in high-energy piping have increased significantly during the second part of the twentieth century, in spite of improved construction procedures and the high quality of materials used. The result has been a grave expansion in the number of fatal disasters and ecological catastrophes, and their harmful social and economic consequences. This trend is apparent from a brief analysis of extensively developing industrial activities in different countries of the world, such as chemical, refinery and gas-treatment enterprises, power and the nuclear power industry. The statistics of failures in these industries show that most of the damage was caused by systems of interacting flaws.

To numerically tackle these problems a previously developed code by the authors, based on the Element Free Galerkin (EFG) solution of systems of strongly interacting static cracks, was modified and adapted for dynamic problems in fracture mechanics. Several numerical examples of single crack propagation under impulse loading are solved. Accuracy of the results is verified comparing several analytical and numerical methods. The developed method is then applied to the physical model of dynamic crack propagation in the field of interacting flaws.

1 Introduction

Dynamic fracture and crack arrest criteria have only begun to appear in the literature. The models of the interaction of flaws under dynamic load, the interaction of a main crack with a system of flaws, and the dynamic growth of a crack in a field of interacting cracks are not well developed. There are no general, reliable, efficient and accurate methods for the numerical solution of these problems.

As result of the lack of reliable experimental methods and procedures for evaluation of stress and strain fields, stress intensity factors and energy release rates, unexpected and rarely predictable failures caused by individual flaws and systems of interacting flaws continue to occur in high-pressure equipment

operating under dynamic loading, especially in enclosed spaces (nuclear reactors, submarines, shuttles). These failures jeopardize operational safety, and can lead to fatal disasters, catastrophes, and social and economical losses.

The problem of single crack behavior under dynamic pulse load was investigated numerically by different authors. Parton and Boriskovsky (1985, [1]), Nakamura, Shih and Freund (1985, [2]) were the first who solved it by the Finite Element method. Later, the problem was analyzed by other numerical methods. Lu, Belytschko and Tabbara in 1995 [3] and Organ in 1996 [4] have applied the Element Free Galerkin method and Chen, Gerlach, and Belytschko (2001, [5]) used the Extended Finite Elements method for the solution of the problem. Techniques of these works and the results of our investigations devoted to the solution of static interacting cracks problems are used here with certain adaptation for the solution of dynamic multi-crack problems. These will be considered below in detail.

2 The EFG Method for Dynamic Linear Elastic Fracture Mechanics

For numerical solution of dynamic linear elastic fracture mechanics problems by the EFG method, the discrete equation is derived from the variational form of the governing equation of motion.

Consider the analytical equation of motion

$$\sigma_{ij,j} + b = \rho \ddot{u}_i, \quad \text{in domain } \Omega \text{ bounded by } \Gamma, \quad (1)$$

where σ_{ij} is the stress tensor, b is the body force and ρ is the material density.

Equation (1) has the following boundary conditions (b.c.) and initial conditions (i.c.):

$$\text{Essential b.c.: } u_i = \bar{u}_i \text{ on } \Gamma_u, \quad (2)$$

$$\text{Natural b.c.: } \sigma_{ij} n_j = \bar{t}_i \text{ on } \Gamma_t, \quad (3)$$

$$\text{Displacement i.c.: } u(x, 0) = u_0(x), \quad (4)$$

$$\text{Velocity i.c.: } \dot{u}(x, 0) = v_0(x), \quad (5)$$

where \bar{u}, \bar{t} are prescribed boundary displacements and tractions respectively, and n is the unit normal vector to Γ .

The variational form of the equation (1) is

$$\int_{\Omega} \rho \delta u \cdot \ddot{u} d\Omega + \int_{\Omega} \sigma^T \delta \varepsilon d\Omega = \int_{\Omega} \delta u \cdot b d\Omega - \int_{\Gamma_t} \delta u \cdot \bar{t} d\Gamma, \quad (6)$$

where δ is the variation operator.

The discrete form of equation (6) is

$$M\ddot{u} + f^{int} = f^{ext}, \quad (7)$$

M is the mass matrix diagonalized by the row-sum method, f^{ext} and f^{int} are the vectors of external and internal forces respectively.

$$M_{II} = \sum_J \int_{\Omega} \rho \phi_I \phi_J d\Omega, \quad (8)$$

$$f_I^{ext} = \int_{\Gamma_t} \phi_I \bar{t} d\Gamma + \int_{\Omega} \phi_I b d\Omega, \quad (9)$$

$$f_I^{int} = \int_{\Omega} B_I^T \sigma d\Omega, \quad (10)$$

where ϕ_I are the EFG shape functions, B_I is a matrix of shape function derivatives:

$$B_I = \begin{bmatrix} \phi_{I,x} & 0 \\ 0 & \phi_{I,y} \\ \phi_{I,y} & \phi_{I,x} \end{bmatrix}. \quad (11)$$

For the time evolution approximation we use the following three schemes: a regular second-order accurate central difference scheme, a fourth-order accurate difference scheme and the Newmark method.

The time evolution approximation by a regular central difference scheme is given by:

$$u_{t+\Delta t} = 2u_t - u_{t-\Delta t} + \Delta t^2 M_t^{-1} (f_t^{ext} - f_t^{int}). \quad (12)$$

We derive the time evolution approximation by a fourth-order accurate scheme from the Taylor series:

$$u_{t+\Delta t} = u_t + \Delta t \dot{u}_t + \frac{\Delta t^2}{2} \ddot{u}_t + \frac{\Delta t^3}{6} u_t^{(3)} + \frac{\Delta t^4}{24} u_t^{(4)} + \dots \quad (13)$$

$$u_{t-\Delta t} = u_t - \Delta t \dot{u}_t + \frac{\Delta t^2}{2} \ddot{u}_t - \frac{\Delta t^3}{6} u_t^{(3)} + \frac{\Delta t^4}{24} u_t^{(4)} + \dots \quad (14)$$

Summarizing (13) and (14) and truncating the series we obtain:

$$u_{t+\Delta t} + u_{t-\Delta t} = 2u_t + \Delta t^2 \ddot{u}_t + \frac{\Delta t^4}{12} u_t^{(4)} + O(\Delta t^6). \quad (15)$$

Then

$$\ddot{u}_t = \frac{u_{t+\Delta t} - 2u_t + u_{t-\Delta t}}{\Delta t^2} - \frac{\Delta t^2}{12} u_t^{(4)} + O(\Delta t^4). \quad (16)$$

The second-order accurate backward difference is used to approximate the fourth-order material derivative u_t , which results in fourth-order convergence for the difference equation.

$$u_t^{\dots} = \frac{2\ddot{u}_t - 5\ddot{u}_{t-\Delta t} + 4\ddot{u}_{t-2\Delta t} - \ddot{u}_{t-3\Delta t}}{\Delta t^2} + O(\Delta t^2). \quad (17)$$

Finally we get the following time evolution rule:

$$u_{t+\Delta t} = 2u_t - u_{t-\Delta t} + \Delta t^2 A_t + \frac{\Delta t^2}{12} (2A_t - 5A_{t-\Delta t} + 4A_{t-2\Delta t} - A_{t-3\Delta t}), \quad (18)$$

where

$$A_t = M_t^{-1} \left(f_t^{ext} - f_t^{int} \right). \quad (19)$$

Another technique that can be used for numerical integration is the two parameter Newmark family of methods. These methods truncate the Taylor series:

$$u_t = u_{t-\Delta t} + \Delta t \dot{u}_{t-\Delta t} + \frac{\Delta t^2}{2} \ddot{u}_{t-\Delta t} + \frac{\Delta t^3}{6} u_{t-\Delta t}^{\dots} + \dots, \quad (20)$$

$$\dot{u}_t = \dot{u}_{t-\Delta t} + \Delta t \ddot{u}_{t-\Delta t} + \frac{\Delta t^2}{2} u_{t-\Delta t}^{\dots} + \dots \quad (21)$$

The parameters β and γ of the Newmark method are defined in following expressions using (20) and (21):

$$u_t = u_{t-\Delta t} + \Delta t \dot{u}_{t-\Delta t} + \frac{\Delta t^2}{2} \ddot{u}_{t-\Delta t} + \beta \Delta t^3 u_{t-\Delta t}^{\dots}, \quad (22)$$

$$\dot{u}_t = \dot{u}_{t-\Delta t} + \Delta t \ddot{u}_{t-\Delta t} + \gamma \Delta t^2 u_{t-\Delta t}^{\dots}. \quad (23)$$

If the acceleration is assumed to be linear then:

$$u_t^{\dots} = \frac{\ddot{u}_t - \ddot{u}_{t-\Delta t}}{\Delta t}, \quad (24)$$

$$u_t = u_{t-\Delta t} + \Delta t \dot{u}_{t-\Delta t} + \left(\frac{1}{2} - \beta \right) \Delta t^2 \ddot{u}_{t-\Delta t} + \beta \Delta t^2 \ddot{u}_t, \quad (25)$$

$$\dot{u}_t = \dot{u}_{t-\Delta t} + (1 - \gamma) \Delta t \ddot{u}_{t-\Delta t} + \gamma \Delta t \ddot{u}_t. \quad (26)$$

Finally,

$$(b_1 M + K) u_t = f_t^{ext} + M (b_1 u_{t-\Delta t} - b_2 \dot{u}_{t-\Delta t} - b_3 \ddot{u}_{t-\Delta t}), \quad (27)$$

$$\ddot{u}_t = b_1 (u_t - u_{t-\Delta t}) + b_2 \dot{u}_{t-\Delta t} + b_3 \ddot{u}_{t-\Delta t}, \quad (28)$$

$$\dot{u}_t = b_4 (u_t - u_{t-\Delta t}) + b_5 \dot{u}_{t-\Delta t} + b_6 \ddot{u}_{t-\Delta t}, \quad (29)$$

where

$$\begin{aligned} b_1 &= \frac{1}{\beta \Delta t^2}, b_2 = -\frac{1}{\beta \Delta t}, b_3 = -\left(\frac{1}{2\beta} - 1\right), \\ b_4 &= \gamma \Delta t b_1, b_5 = 1 + \gamma \Delta t b_2, b_6 = \Delta t (1 + \gamma b_3 - \gamma). \end{aligned} \quad (30)$$

The method is unconditionally stable if

$$2\beta \geq \gamma \geq \frac{1}{2}, \quad (31)$$

and there is energy damping if

$$\gamma > \frac{1}{2}. \quad (32)$$

It should be noted that in the dynamic problems the weight functions and their domains of influence are time dependent. That leads to the time dependence of the shape functions. Since the time dependence of the shape functions and their derivatives can not be analytically expressed for the case of arbitrary dynamic fracture, these functions should be updated with every time step, based on the new crack geometry and the updated weight function. Next we will use previously described methods for the numerical solution of the dynamic problems of our interest.

3 Solution of Multi-Crack Problems by the EFG Method

Currently, the solution of problems with many cracks by a finite element method requires enormous mesh refinement near each crack tip, including the embedding of many singular elements. When using meshless methods and the EFG method in particular, many additional nodes should be added around and between the cracks and the nodal domain of influence should be lowered significantly. As a result a huge computational effort is needed for the solution.

To overcome the problem, we developed an algorithm for the construction of weight functions to handle strongly interacting multi-crack, where the distance between cracks can be smaller than the domain of influence of the nodes [6]. This algorithm modifies the diffraction method [7] so that it can characterize simultaneously all crack tips located in the nodal domain of influence. The same algorithm can be used to modify other methods for construction of weight functions. Among these are methods based on the modification of the weight function shape near crack tips, such as transparency [7] and visibility methods [8]. The algorithm was presented for example of the diffraction method in [6]. We call this method the *multiple crack weight* (MCW) method.

This section presents the reliability and accuracy of the EFG method together with the MCW method for the solution of multiple cracks problems. Numerical examples of interacting and intersecting cracks are calculated in

terms of the stress intensity factors and compared to available reference solutions provided by other numerical methods. Problems about star-shaped cracks under bi-axial static load are chosen to illustrate the main aspects of solution of multiple crack problems. The convergence of the stress intensity factors as a function of number of nodes is analyzed and discussed.

In all the calculations the nodal distribution was regular with additional nodes along the cracks surfaces, star-shaped array of nodes around of the free tips of the cracks and an additional node at the free tips of the cracks. The radius of the outer ring of star-shaped additional nodes was equal to 0.75 of the distance between regular nodes. The regular nodal distribution was used as a mesh for the numerical integration by the Gauss quadrature rule with 12x12 Gauss quadrature points in each cell. The fully enriched basis [9] was coupled with a linear basis. The outer radius of the enrichment was smaller than the outer radius of the star-shaped additional nodes. A plane strain condition was assumed.

Six intersecting cracks were used to model a star-shaped crack (Fig. 1a). The normalized stress intensity factors $F_I^A = K_I^A/\sigma\sqrt{\pi a}$, $F_I^B = K_I^B/\sigma\sqrt{\pi a}$ and $F_{II}^B = K_{II}^B/\sigma\sqrt{\pi a}$ were calculated using the domain form of the interaction integral for $a/W=0.5$ and several ratios of a/h , where W is the half width of the specimen, a is the crack length and h is the average nodal spacing. The results presented in Fig. 2 show the convergence of the solution as the mesh is refined. The stress intensity factors are oscillating while they converge to their limiting values. The amplitude of the oscillations vanishes as the ratio a/h increases. The relative differences between the stress intensity factors, F_I^A , F_I^B , F_{II}^B calculated with $a/h=5$ mesh and those calculated with $a/h=10$ mesh were 0.23%, 0.2%, 0.75% respectively.

Comparing these results with the reference solutions [10,11], one sees that the accuracy of the solution is acceptable even for the relatively small ratio of $a/h=5$ (mesh with 21x21 regular nodes) and that the results agree satisfactorily with the references in [10,11] (Table 1, case $a/W=0.5$). This is despite the fact that the small regular nodal distribution can not match inclined crack lines properly, several cells of the integration mesh are crossed by cracks and two crack tips are in the nodal domain of influence of many nodes. This demonstrates that the modified EFG method combined with MCW method is able to solve accurately multiple crack problems with relatively small nodal distributions.

The same mesh distributions that were used for the cross-shaped crack problem were used to solve the star-shaped crack problem for different a/W ratios. The calculated normalized stress intensity factors (Table 1) were compared with those calculated by X-FEM in [10] for two different meshes distributions (Table 1 ref 1 and ref 2) and by Cheung et al in [11] (Table 1 ref 3). Our results show good agreement with the reference results and are closer to those provided by X-FEM than to results of Cheung et al.

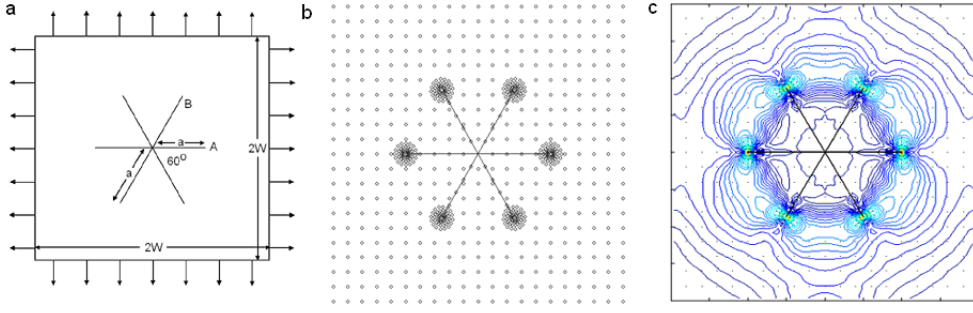


Fig. 1. Finite-size plate with star-shaped crack under bi-axial loading (a). Mesh distribution for $a/W=0.5$ (b). Von Mises stress distribution for $a/W=0.5$ (c).

Table 1. Normalized stress intensity factors for the problem in Fig. 1.

		F_I	F_I ref 1	F_I ref 2	F_I ref 3	$E_1, \%$	$E_2, \%$	$E_3, \%$
$a/W = 0.2$	F_I^B	0.7690	0.7683	-	0.7578	0.09	-	1.48
$a/W = 0.2$	F_{II}^B	0.0007	0.0005	-	0.0004	*	-	*
$a/W = 0.2$	F_I^A	0.7691	0.7670	0.7746	0.7570	0.27	0.71	1.60
$a/W = 0.3$	F_I^B	0.7994	0.7983	0.7973	0.7884	0.14	0.26	1.40
$a/W = 0.3$	F_{II}^B	0.0020	0.0021	0.0021	0.0022	*	*	*
$a/W = 0.3$	F_I^A	0.7970	0.7931	0.7942	0.7846	0.49	0.35	1.58
$a/W = 0.4$	F_I^B	0.8527	0.8466	0.8466	0.8365	0.72	0.72	1.94
$a/W = 0.4$	F_{II}^B	0.0077	0.0080	0.0064	0.0070	*	*	*
$a/W = 0.4$	F_I^A	0.8352	0.8287	0.8332	0.8255	0.78	0.24	1.18
$a/W = 0.5$	F_I^B	0.9232	0.9255	0.9208	0.9087	0.25	0.26	1.60
$a/W = 0.5$	F_{II}^B	0.0201	0.0184	0.0168	0.0168	*	*	*
$a/W = 0.5$	F_I^A	0.8921	0.8864	0.8928	0.8815	0.64	0.08	1.20
$a/W = 0.6$	F_I^B	1.0405	1.0445	1.0401	1.0182	0.38	0.04	2.19
$a/W = 0.6$	F_{II}^B	0.0451	0.0364	0.0350	0.0388	*	*	*
$a/W = 0.6$	F_I^A	0.9749	0.9673	0.9760	0.9758	0.79	0.11	0.09
$a/W = 0.7$	F_I^B	1.2384	1.2367	1.2369	1.1936	0.14	0.12	3.75
$a/W = 0.7$	F_{II}^B	0.0622	0.0593	0.0614	0.0529	*	*	*
$a/W = 0.7$	F_I^A	1.1022	1.0971	1.1120	1.1142	0.46	0.88	1.08
$a/W = 0.8$	F_I^B	1.5577	1.5624	1.5593	-	0.30	0.10	-
$a/W = 0.8$	F_{II}^B	0.0804	0.0864	0.0826	-	*	*	-
$a/W = 0.8$	F_I^A	1.3454	1.3423	1.3581	-	0.23	0.94	-
$a/W = 0.9$	F_I^B	2.1605	2.1927	2.1659	-	1.47	0.25	-
$a/W = 0.9$	F_{II}^B	0.0906	0.0868	0.088	-	*	*	-
$a/W = 0.9$	F_I^A	1.9146	1.9037	1.9578	-	0.57	2.21	-

$E_{1,2,3}$ represent the percent difference of normalized stress intensity factors F_I^A , F_I^B with reference solutions ref 1,2,3.

* The percent difference is not representative in this case since the calculated and reference values of F_{II}^B are small or close to zero. We note that in this case there is even a significant percent difference between the three reference solutions.

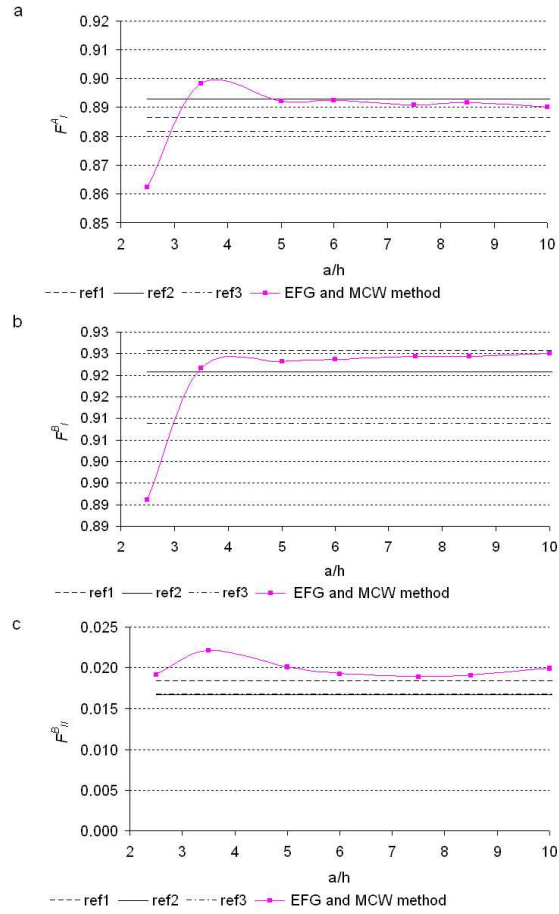


Fig. 2. Convergence of the normalized stress intensity factors (a) F_I^A , (b) F_I^B , (c) F_{II}^B as a function of the average nodal spacing. The results of ref 2 and ref 3 are identical in (c).

The results show that the MCW method allows the solution of strongly interacting cracks without enormous mesh refinement and reduces significantly the computational efforts. Thus in different numerical examples the computational time was two to four time shorter when using the EFG method with MCW method because smaller nodal distributions were required compared with the standard EFG method for obtaining accurate results.

4 Individual Crack Subjected to Pulse Loading

4.1 Introduction

In this section we consider the physical model of Cherepanov [12] which describes crack behavior under dynamic pulse load and discuss the accuracy of the numerical solution by the EFG method. This model considers semi-infinite crack development in an infinite body subjected to dynamic impulse and includes several stages:

- The concentration of the stress around the crack tip and the increasing of stress intensity factor.
- Initiation of a crack's propagation and subsequent crack elongation with increasing speed.
- Decelerating and arresting of a crack after removal of applied forces.

Cherepanov solved analytically the stress intensity factor for the stationary crack under the pulse of a rectangular pulse of finite duration $\sigma_y(t)$ applied normally to the crack plane:

$$\sigma_y(t) = \sigma_0 [H(t) - H(t - T)], \quad (33)$$

where σ_0 is the pulse amplitude; T is the pulse duration; H is the Heaviside function.

According to his solution, the stress intensity factor, K_{st} of static crack subjected to impulse loading is:

$$K_{st}(t) = \frac{4\sigma_0 c_2}{c_1 \sqrt{\pi c_1}} \sqrt{c_1 - c_2} \left[\sqrt{t} H(t) - \sqrt{t - T} H(t - T) \right], \quad (34)$$

where c_1 and c_2 are dilatation and shear wave speeds, respectively.

The corresponding to K_{st} energy release rate G_{st} in condition of opening mode of fracture is:

$$G_{st} = \frac{K_{st}^2}{E'}, \quad (35)$$

where $E' = E$ for plane stress and $E' = E/(1 - \nu)^2$ for plane strain problems, where E is the elastic modulus and ν is the Poisson ratio.

The energy release rate G of propagating crack with velocity \dot{l} , can be obtain from the expression provided by Freund [13]:

$$G(t, \dot{l}) = g(\dot{l}) G_{st}(t), \quad (36)$$

where

$$g(\dot{l}) = 1 - \dot{l}/c_R, \quad (37)$$

and c_R is the Rayleigh wave speed. The velocity of the crack propagation is obtained from:

$$\dot{l} = c_R (1 - G_{critical}/G_{st}(t)). \quad (38)$$

For numerical solution of the energy release rate, we use a domain form of path-independent integral proposed by Moran and Shih [14]:

$$G = - \int_A ((W + L) \delta_{1j} - \sigma_{ij} u_{i,1} m_j) q, j dA - \int_A (\rho \dot{u}_i \dot{u}_{i,1} - \rho \ddot{u}_i u_{i,1}) q dA, \quad (39)$$

where q is a weight function that equals one on the inner boundary of the integral domain, zero on the outer boundary and is arbitrary elsewhere.

We assume that Cherepanov's model satisfies the real conditions of fracture in high energy equipment. Nevertheless, the further research of the phenomenology of dynamic fracture under pulse loading especially for the case of interacting cracks requires the analysis of the cracks characteristics such energy release rates, calculation of the direction of the crack propagation and the dynamic stress and strain fields.

4.2 Analysis of accuracy

In this section we discuss the accuracy of the EFG method for the solution of static and propagating individual cracks under impulse load. For this we solve the numerical example of a finite plate with width 10m and height 4m and an edge crack with length of 5m subjected to impulse load as illustrated in Fig. 3. The time of the problem is limited to the time that it takes for the stress wave to pass down to the bottom boundary, reflect from its surface and then arrive back to the crack line, $t=3H/c_1$, where H is the half of specimen's height. For longer times the comparison of the numerical solution with the existing analytical solutions [12,13] is not valid.

The dynamic loading was created by an incident tensile pulse with amplitude $\sigma_0=1000$ N/m² suddenly applied at the top boundary of the stress free specimen with the following material properties: $E = 211 \cdot 10^9$ N/m², $\rho=7800$ kg/m³, $\nu=0.3$. A plane strain condition was assumed.

The selected EFG scheme includes a regular nodal distribution, a 4x4 Gauss quadrature rule, and linear basis functions. The time step used for numerical integration was calculated according to the Courant condition, where the critical time step is $dt_c = h/c_1$, and h is the minimum nodal spacing. The time evolution approximation was done using the central difference scheme.

For the analysis of the numerical scheme we started with two examples of the crack behavior under impulse loading:

- Crack remains stationary for the entire calculation.
- Crack remains stationary until $t_1 = 1.5H/c_1$ and then starts to propagate with constant velocity $V = 0.4c_2$. We note that the analytical value of the energy release rate at $t_1 = 1.5H/c_1$ is equal to $0.475G^* = 4.5 \cdot 10^{-6} Pa \cdot m$, where $G^* = H\sigma_0^2/E$. We will assume later in numerical examples that the critical energy release rate G_{1c} is equal $0.475G^*$.

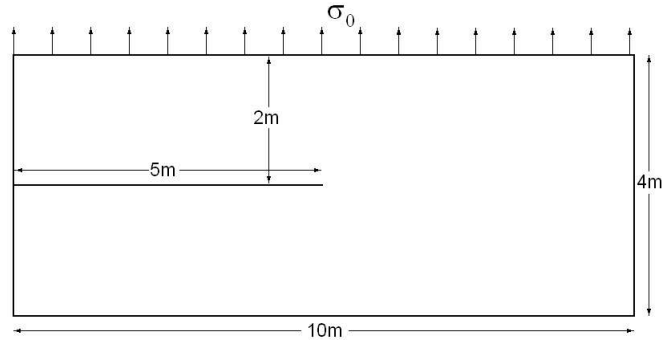


Fig. 3. Edge crack in the specimen modeling infinite plate subjected to pulse loading.

In both cases the energy release rates were calculated and compared to the analytical values which were obtained from the solution of Cherepanov [12] and Freund [13]. It should be noted that the energy release rate is a linear function of time in this example. Later this characteristic will be used in the accuracy analysis.

Several nodal distribution were used (120x48, 180x72, 240x96, 300x120 for the first case of stationary crack and 120x48, 240x96 for the second case of a stationary and then propagating crack) to show the convergence of the solution as a function of nodal density. To satisfy the Courant condition for all nodal densities we selected the time step equal to $0.5 \cdot 10^{-6}$ sec.

The analysis of the results concerning the first case showed that the energy release rate is growing smoothly but oscillating along the analytical line (Fig. 4a, b, c, d) from the moment when the stress wave arrives at the crack line ($t = H/c_1$). For the higher nodal densities the amplitude of the oscillation is decreases. To assess the accuracy of the solution quantitatively, we propose to use several statistical tools. Thus, we calculate the average, E and the standard deviation, S of the relative errors in the energy release rates calculated for every time step, and the coefficient of correlation, R between the energy release rates and time.

Since the analytical energy release rate is a linear function of time, the coefficient of correlation was used as a tool to assess the linear dependence of the numerically calculated energy release rate on time. The standard deviation is calculated to characterize the dispersion of relative errors between the calculated energy release rates and the analytical values. Thus, one can see in Table 2 that the coefficient of correlation, R converges to 1 as the nodal density increased and the linear character of the energy release rate in time improves. At the same time, the standard deviation and the average error of the numerical results decrease.

In the second case, after the time $t = 1.5H/c_1$ when the crack starts to propagate at a constant velocity one can see that the solution oscillates with higher amplitudes compared to the case of a static crack, see Fig. 4e, f. The drop in the energy release rate predicted by the analytical solution of Freund [13] at $t = 1.5H/c_1$ is clearly seen in our results. For the higher nodal discretization this drop was sharper.

Table 2. Average, E , standard deviation, S , and coefficient of correlation, R , of the relative error in the energy release rate.

Nodal distribution	E	S	R
120x48	0.07046	0.14017	0.99899
180x72	0.05530	0.12307	0.99947
240x96	0.04768	0.11322	0.99963
300x120	0.04008	0.04008	0.99977

To analyze the solution's oscillations we conducted several investigations. It was established, that the solution with a higher order Gauss quadrature for numerical integrations of the mass matrix and f^{ext} , f^{int} , and energy release rate did not yield significant improvement, leaving the same character of oscillations. Different sizes of energy release rate domain also did not change the results, proving that the dynamic energy release rate calculated by (39) is independent of the domain size. Decreasing the time step, application of enrichment techniques and a fourth-order accurate scheme did not show any obvious differences in the results. We therefore concluded that the accuracy is more sensitive to the nodal density than to other parameters of the appropriate numerical scheme selected before. In our opinion one of the possible ways to reduce the oscillations for dynamic crack is to add the moving star-shaped arrays of nodes around the tip of the developing crack.

In addition, the Newmark family of methods was used for numerical integration. Solving the energy release rate for static cracks with different values of β and γ parameters, it was established that for $\beta = 1/4$ and $\gamma = 3/4$ the solution is more accurate and smoother, Fig. 5a,b. Thus, for 120x48 nodal distribution, E equals 0.06682, $S = 0.13845$ and $R = 0.99956$, and for a 180x72 nodal distribution, $E = 0.04838$, $S = 0.11549$ and $R = 0.99978$.

This Newmark scheme induces small energy damping, which improves the solution of this particular problem. However, it should be used with care in other problems. So far there is no well established proof that the procedure can provide an accurate solution for multiple crack problems, where small solution oscillations could be the result of crack interactions and not due to numerical error.

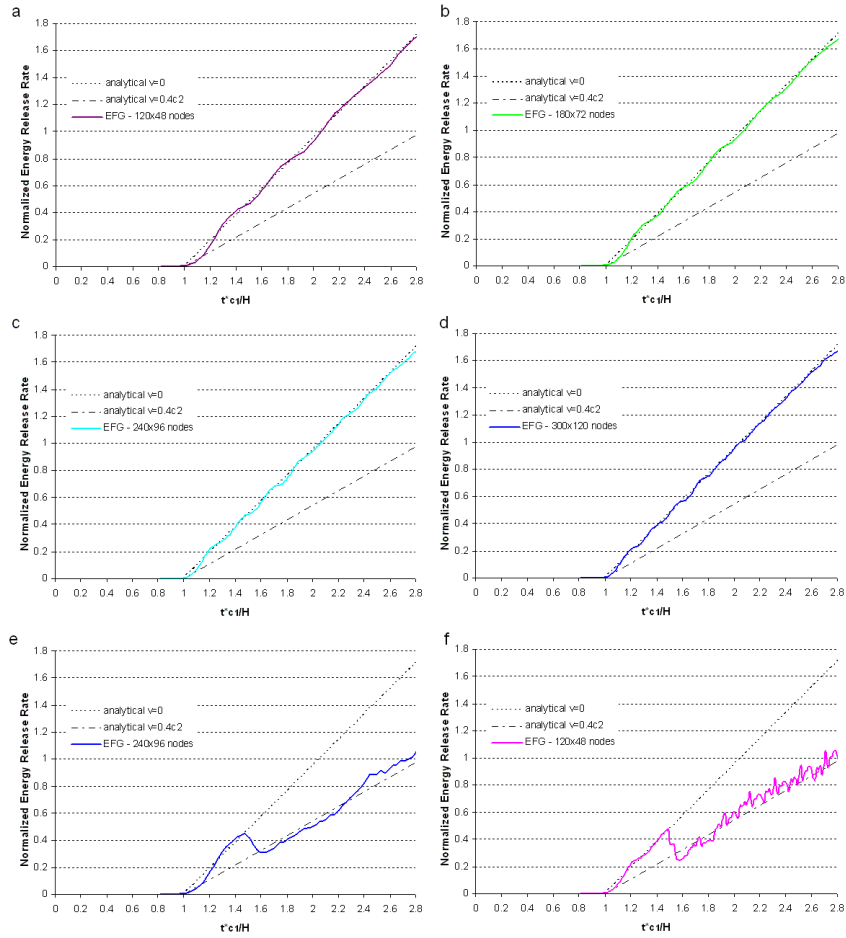


Fig. 4. Energy release rates for the static crack and static and then dynamic crack propagating at constant velocity, normalized by $H\sigma_0^2/E$.

We note that the level of the oscillations of the energy release rate calculated by (39) in Fig. 4e,f are lower than found in other works [15],[16]. In [15] it was noted that "the oscillations for the moving cracks coincide with the number of nodes passed during propagation; the peaks occur just before the crack tip passes a node". Therefore it is important to take into consideration the character of the oscillations when analyzing different physical phenomena of propagating cracks to prevent misleading results. Next we shall apply the considered EFG scheme with the central difference scheme to the numerical calculation of Cherepanov's model.

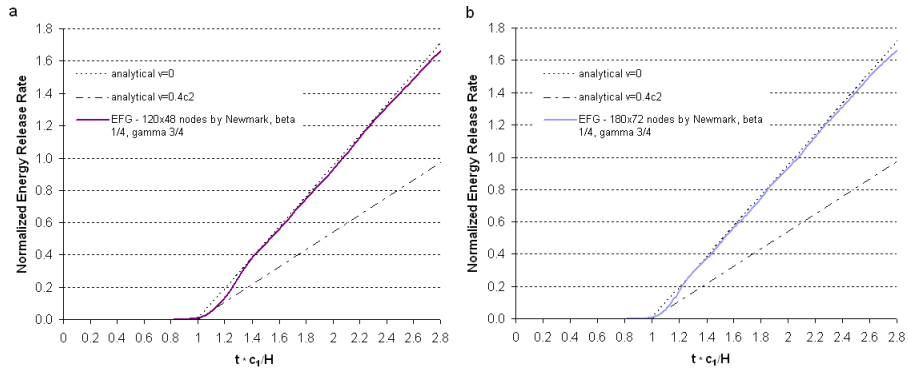


Fig. 5. Energy release rates normalized by $H\sigma_0^2/E$ for a static crack subject to pulse loading calculated by Newmark method with $\beta = 1/4$ and $\gamma = 3/4$.

5 Main Crack Propagation in a Field of Interacting Flaws under Dynamic Pulse Loading

Below we shall consider the typical case of failure which occurs in high-pressure equipment - main crack propagation in a field of interacting flaws under influence of pulse load of finite duration. We use the same specimen for the modeling of the problem as in the previous section. The applied impulse has a finite duration equal H/c_1 . The geometry of the main crack and the system of micro-cracks is shown in Fig. 6. In addition we solve the problem of the single main crack propagation without micro-cracks for the same specimen and pulse load. Three stages of Cherepanov’s model were analyzed and compared to the case of a single crack problem to establish the effect of a system of micro-cracks on the energetic characteristics of the main crack.

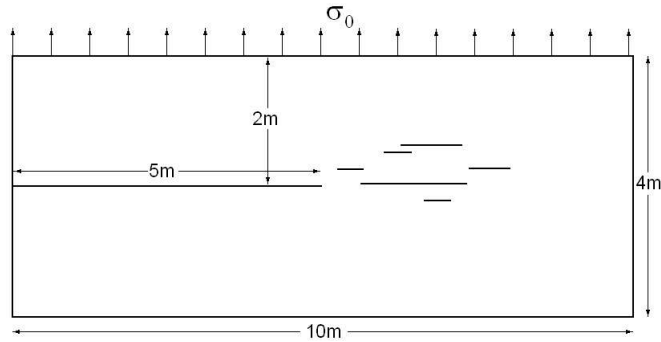


Fig. 6. Main crack interacting with system of micro-cracks in the plate modeling infinite plate subjected to tensile pulse loading.

The calculation established that initially a pulse load creates a uniformly distributed stress field that moves toward the main crack (Fig. 7a). Later, when the stress wave arrives at time H/c_1 to the main crack line, the tip of the main crack starts to accumulate and concentrate energy (Fig. 7b). As a result the energy release rate grows linearly (Fig. 7f). There is no clear indication of interaction between the main crack and the system of micro-cracks. The energy release rate of the main crack is not different from the case of the single crack. However, as the stress intensity continues to rise around the tip of the main crack and system of micro-cracks, the interaction effect begins at approximately $t = 1.3H/c_1$. The energy release rate increases relative to the case of the single main crack, indicating that an amplification effect is taking place.

In the zone where the system of cracks is located there are clear signs of a non-uniform stress concentration (Fig. 7b). Some of the cracks concentrate the energy intensively, while others, shielded by external cracks from the pulse stress wave, which is moving in their direction, and do not accumulate stresses. The combined stress field around the system of the cracks is extremely anisotropic.

The main crack starts to propagate when the energy release rate of the main crack exceeds its critical value (Fig. 7f). The initiation of crack growth occurs earlier than in the case of a single crack due to the stress amplification effect. From the beginning, the crack propagated with higher velocity and elongates faster relative to the case of a single crack without the system of micro-cracks (Fig. 7g, h). As the distance between the main crack and the system of micro-cracks decrease, the amplifying effect increases and the redistribution of the stress field becomes obvious (Fig. 7c, d). The maximum velocity that the main crack interacting with the system of micro-cracks reaches is 1050m/s, while for the single crack it is 700m/s. The stress field around the tip of the main crack starts to interact with the stress field of system of micro-cracks and the redistribution of the stress field becomes obvious (Fig. 7c, d), indicating dynamic interaction.

The main crack decelerates as the impulse interrupts at time $t = 2H/c_1$. Its velocity and the rate of its elongation decrease (Fig. 7g, h). However, the energy accumulated in the specimen supports fracture development and the main crack continues its motion toward the micro-crack system. It increases the interaction effect and as a result an interesting phenomenon occurs: the main crack continues to propagate for a longer distance compared with the case of a single crack despite the absence of load on the specimen's boundaries (Fig. 7h). The deceleration of a main crack (Fig. 7g) continues until approximately $t=3H/c_1$ relative to $t=2.14H/c_1$ in the case of a single crack.

One can observe oscillations in the numerical results of the velocity in Fig. 7g after $t=2H/c_1$. As in the case of a single crack propagating with constant velocity considered previously, the peaks occur just before a crack tip

passes a node. However, the amplitude of the velocity oscillations attenuates indicating further crack arrest. It should be noted, that the character of the oscillation does not adversely affect the main physical phenomena observed in this example - the main crack elongates for larger lengths if interacting with other cracks. We wish to stress that the same level of oscillations appears in the velocity of a moving single crack in [15].

After all these, the results of the analysis showed us that:

- The energy release rate varies and depends strongly on the position of the applied dynamic load, the direction of the stress wave propagation and on the mutual position of the tip of the main crack and the system of cracks and their sizes.
- The crack may start to propagate earlier if interacting with other flaws.
- The interaction of the main crack with the system of micro-cracks changes the velocity of the main crack propagation.
- The process of crack development under pulse loading and crack deceleration can take longer due to the stress amplification effect.
- The main crack may elongate for larger lengths if interacting with other cracks. This may lower the component's life time subjected to impulse loading.

In the above, we forced the main crack to propagate linearly and the system of micro-cracks was assumed to be static. This was done in order to:

- Compare the behavior of a single main crack undergoing pulse load and when a main crack interacting with a system of micro-cracks.
- Investigate how a system of micro-cracks located at different distances from the tip of the main crack changes the energy release rate, velocity, energy flow density distribution around the main crack.

We will consider below the problem where the main crack and micro-cracks inside of the system of flaws start to propagate at a constant velocity equal to $0.4c_2$ when their energy release rates exceed the critical value G_{1c} , under the influence of a pulse load. We postulate that cracks propagate according to the maximum principal stress criterion.

The results of the calculations show that:

- When the accumulated energy at the cracks tips becomes critical and cracks start to propagate, the interaction effect is taking place. This result in the local redistribution of stresses at the tips of the cracks. This changes the direction of propagation of the main crack and of individual cracks of the system of micro-cracks.

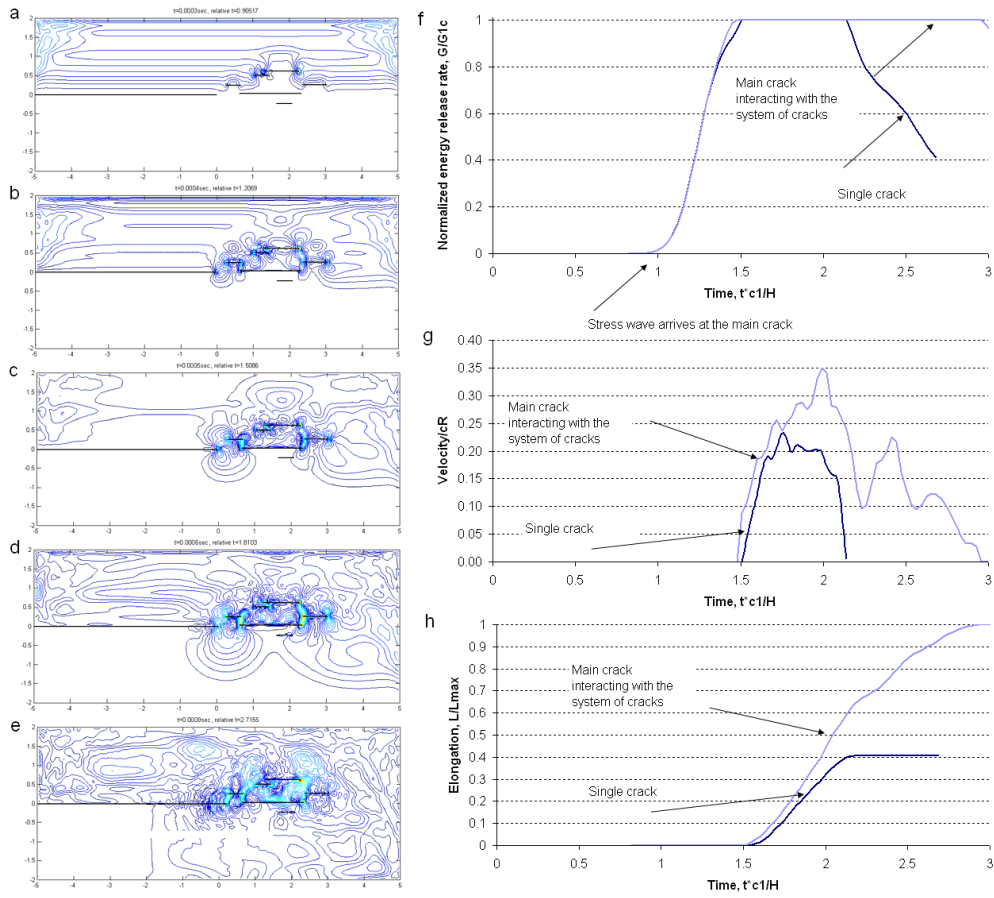


Fig. 7. (a)-(e) Von-Mises stress distribution for the main crack interacting with the system of micro-crack and (f) energy release rate, (g) velocity and (h) elongation of the propagating main crack interacting with a system of micro-cracks compared with a single main crack.

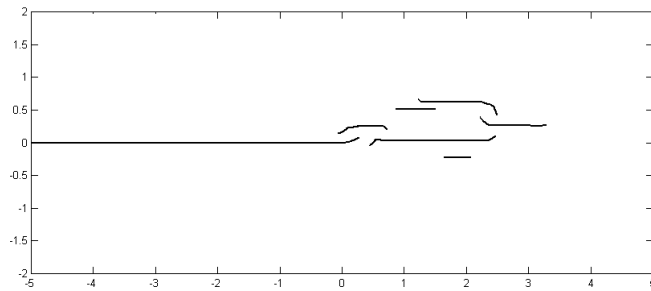


Fig. 8. Main crack and micro-cracks interacting and propagating with changing direction.

- Cracks initially located perpendicular to the applied forces do not propagate linearly. The trajectory of the growing cracks is presented in Fig. 8.
- Some micro-cracks that accumulate more energy start to propagate early and pass through longer distances than others do.
- Micro-cracks that are shielded by other cracks from the pulse stress wave do not propagate.
- Cracks that are located parallel to each other tend to increase the distance between themselves to reduce the shielding effect and then propagate parallel to each other.
- Propagating cracks which are collinear or shifted relative to each other, including the main crack tend to coalesce similar to what was observed in of metallurgical investigations.
- As a result of the main crack's propagation and interaction with the system of developing micro-cracks, they tend to coalesce with each other to create one macro-flaw.

6 Conclusions

The physical models and numerical methods for investigating individual and interacting randomly dispersed cracks were elaborated and developed. We evaluated their danger level, and the velocity and the direction of a main propagating in a system of interacting cracks. Phenomena of dynamic crack interactions were investigated. These in particular included:

A special, the multiple crack weight (MCW), method for constructing weight functions for multi-crack problems was created. This defines the weight functions around cracks in such a way that they can simultaneously characterize all the crack tips present in the nodal domain of influence. Thus it allows the solution of strongly interacting static and dynamic cracks without enormous mesh refinement and reduces significantly the computational efforts.

The results of the calculated numerical examples show that the new method enables an accurate and reliable solution for static and dynamic strongly interacting cracks problems with relatively small nodal densities. There was less than 0.5% difference between the calculated and at least one of the three corresponding reference values of normalized stress intensity factors F_I^A and F_I^B in all cases, except one for F_I^A and one for F_I^B .

A number of numerical examples of individual interacting cracks undergoing pulse load were solved by the EFG method using different time evolution approximation techniques. The results of the calculations were analyzed. Satisfying accuracy of the solution of numerical examples was achieved compared with analytical solution and the results of other numerical methods.

The problem of main crack propagation in a field of interacting micro-cracks was solved. The analysis has shown that the character of the interac-

tion depends strongly on the position of the applied pulse load, the direction of the stress wave propagation and on the position of the cracks, and their orientation and distance from each other within the system. The interaction of cracks can result in an increase of energy release rate for some of them and lead to their future propagation. Main crack may start to propagate earlier if interacting with other flaws. The interaction of main crack with a system of micro-cracks changes the velocity of its propagation. The process of crack development under pulse loading and crack deceleration can take longer due to the stress amplification effect. Main crack may elongate for longer lengths, when it interacts with other cracks.

References

1. Parton, V.Z. and Boriskovsky, V.G., "Dynamic Fracture Mechanics", Moscow, Mashinostroenie, 1985.
2. Nakamura, T., Shih, C.R. and Freund, L.B., "Computational Methods Based on an Energy Integral in Dynamic Fracture", *International Journal of Fracture*, Vol. 27, 1985, pp. 229-243.
3. Lu, Y.Y., Belytschko, T. and Tabbara, M., "Element-Free Galerkin Methods for Wave Propagation and Dynamic Fracture", *Computer Methods in Applied Mechanics and Engineering*, Vol. 126, 1995, pp. 131-153.
4. Organ, D.J., "Numerical Solutions to Dynamic Fracture Problems Using the Element-Free Galerkin Method" *Ph.D. Thesis*, Northwestern University, 1996.
5. Chen, H., Gerlach, C. and Belytschko, T., "Dynamic Crack Growth with X-FEM" *Presentation*, Dear Born, MI, August 3, 2001.
6. Muravin, B., Turkel, E., "Advance Diffraction Method as a Tool for Solution of Complex Non-Convex Boundary Problems. Implementation and Practical Applications". *Lecture Notes in Computational Science and Engineering: Meshfree Methods for Partial Differential Equations*, Vol. 26, Springer, 2002, pp. 307-317.
7. Organ, D.J., Fleming M.A., and Belytschko T., "Continuous Meshless Approximations for Nonconvex Bodies by Diffraction and Transparency." *Computational Mechanics*, Vol. 18, 1996, pp. 225-235.
8. Belytschko, T., Lu Y.Y., and Gu L., "Element-Free Galerkin Methods." *International Journal for Numerical Methods in Engineering*, Vol. 37, 1994, pp. 229-256.
9. Fleming, M., Chu Y., Moran B., and Belytschko T., "Enriched element free Galerkin methods for crack tip fields". *International Journal for Numerical Methods in Engineering*, Vol. 40, 1997, pp. 1483-1504.
10. Daux, C., Moes, N., Dolbow, J., Sukumar, N. and Belytschko, T., "Arbitrary branched and intersecting cracks with the extended finite element method." *International Journal for Numerical Methods in Engineering*, Vol. 48, 2000, pp. 1741-1760.
11. Cheung, Y., Wang, Y. and Woo, C., "A general method for multiple crack problems in a finite plate." *Computational Mechanics*, Vol. 10, 1992, pp.335-343.
12. Cherepanov, G.P., "Mechanics of Brittle Fracture" /in Russian/, Moscow, Nauka, 1974, 640p.

13. Freund, L.B., "Dynamic Fracture Mechanics", Cambridge University Press, Cambridge, 1990, 581p.
14. Moran, B. and Shih, C.F., "Crack Tip and Associated Domain Integrals from Momentum and Energy Balance", *Engineering Fracture Mechanics*, Vol. 27, No. 6, 1987, pp. 615-641.
15. Organ, D.J., "Numerical Solutions to Dynamic Fracture Problems Using the Element-Free Galerkin Method" *Ph.D. Thesis*, Northwestern University, 1996.
16. Chen, H., Gerlach, C. and Belytschko, T., "Dynamic Crack Growth with X-FEM" *Presentation*, Dear Born, MI, August 3, 2001.

Index

energy release rate, 1

interacting flaws, 1

main crack, 1

micro-cracks, 14

multiple crack weight, 5

pulse load, 9

